

Language Models Resist Alignment: Evidence From Data Compression

Jiaming Ji*, Kaile Wang*, Tianyi Qiu*, Boyuan Chen*, Jiayi Zhou*, Changye Li,
Hantao Lou, Josef Dai, Yunhui Liu, and Yaodong Yang†

Peking University

*{jiang.ji, wkl, tianyi.qiu, cbylll, gaiejj}@stu.pku.edu.cn

†yaodong.yang@pku.edu.cn

Abstract

Large language models (LLMs) may exhibit unintended or undesirable behaviors. Recent works have concentrated on aligning LLMs to mitigate harmful outputs. Despite these efforts, some anomalies indicate that even a well-conducted alignment process can be easily circumvented, whether intentionally or accidentally. Does alignment fine-tuning yield have robust effects on models, or are its impacts merely *superficial*? In this work, we make the first exploration of this phenomenon from both theoretical and empirical perspectives. Empirically, we demonstrate the *elasticity* of post-alignment models, *i.e.*, the tendency to revert to the behavior distribution formed during the pre-training phase upon further fine-tuning. Leveraging compression theory, we formally deduce that fine-tuning disproportionately undermines alignment relative to pre-training, potentially by orders of magnitude. We validate the presence of *elasticity* through experiments on models of varying types and scales. Specifically, we find that model performance declines rapidly before reverting to the pre-training distribution, after which the rate of decline drops significantly. Furthermore, we further reveal that *elasticity* positively correlates with the increased model size and the expansion of pre-training data. Our findings underscore the need to address the inherent *elasticity* of LLMs to mitigate their resistance to alignment.

1 Introduction

Large language models (LLMs) have shown remarkable capabilities (Achiam et al., 2023). However, due to the inevitable biases and harmful content present in training datasets (Bai et al., 2022a; Ji et al., 2024; Qian et al., 2024), LLMs often exhibit behaviors that deviate from human intentions, a phenomenon we refer to as *model misalignment*.

*Equal contribution, corresponding author.

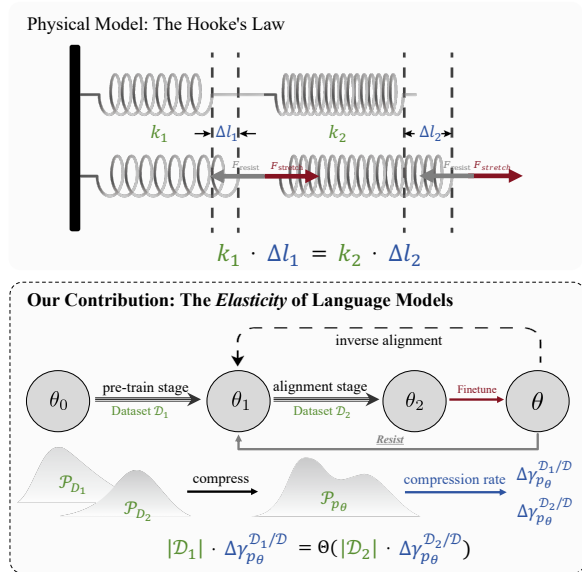


Figure 1: **The Elasticity of Language Models.** When language models undergo fine-tuning perturbations, the change in normalized compression rates ($\Delta\gamma_{p_\theta}^{D_i/D}$) and the dataset volume ($|\mathcal{D}_i|$) across datasets follows an inverse proportionality law akin to the relationship between spring deformation (Δl_i) and stiffness (k_i) in coupled springs. We conjecture that the *elastic* of language models causes language models to resist alignment, enabling the possibility of *inverse alignment*.

Training-based alignment methods, including supervised fine-tuning (SFT), reinforcement learning with human feedback (RLHF) (Ouyang et al., 2022), and other derivatives (Rafailov et al., 2024; Bai et al., 2022b; Lee et al., 2023; Gulcehre et al., 2023; Dong et al., 2023; Xiong et al., 2024; Li et al., 2023), are the dominant approaches for aligning models. These methods aim to optimize model behavior by rejecting harmful distributions, ensuring LLMs remain consistent with human intentions and values (Ji et al., 2023; Casper et al., 2023).

However, these alignment methods do not truly penetrate the model representations but merely perform *superficial alignment* (Qi et al., 2024a; Cohen

et al., 2024; Wen et al., 2024). Recent studies have shown that highly safety-aligned models can become unsafe again with minimal fine-tuning (Yang et al., 2023b; Zhou et al., 2024). Furthermore, fine-tuning aligned LLMs on non-malicious datasets may also weaken models’ safety mechanisms (Qi et al., 2024a; Jain et al., 2023).

Why is alignment so fragile?

In this work, we make the first exploration of the possible mechanism behind the counterintuitive phenomenon: the existence of an alignment resistance mechanism in language models. This mechanism may limit the alignment process of LLMs to superficial adjustments. It could allow the reversal or revocation of alignment through a series of technical measures, a concept we refer to as *inverse alignment*. What drives language models to resist alignment? How does this mechanism lead to *inverse alignment*? Our key contributions are summarized as follows:

- **(Phenomenon)** We uncover that language models exhibit *elasticity*, as illustrated in Figure 1 and Theorem 3.2. It encompasses *resistance*: pre-trained models tend to retain their original distribution; and *rebound*: the deeper alignment of models, the faster they return to the pre-trained distribution under reverse finetuning. Moreover, The model’s change in compression rates $\Delta_{\gamma_{p_{\theta}}^{\mathcal{D}_i/\mathcal{D}}}$ across different datasets is inversely proportional to their sizes $|\mathcal{D}_i|$, which is analogous to the deformation behavior of a series of springs, as illustrated in Section 3.3.
- **(Mechanism)** We systematically model the training and alignment process of language models through compression theorem, as detailed in Section 2.2. We elaborate on the compression protocol of language models to explore their training and alignment processes, laying a foundation for subsequent research on *elasticity*.
- **(Validation)** We experimentally observe consistent *resistance* and *rebound* phenomena across various LLMs, as detailed in Section 4. This highlights the universality of *elasticity* and the need for systematic approaches to achieve robust and deep alignment.

2 What is Elasticity?

In this section, we introduce the definition of language model *elasticity* and the compression theory

tools used in the study. We first review the training alignment objective and the compression theorem.

2.1 Preliminaries

Pre-training. During pre-training, an LLM acquires foundational language comprehension and reasoning abilities by processing vast quantities of unstructured text. The pre-train loss $\mathcal{L}_{\text{PT}}(\theta; \mathcal{D}_{\text{PT}})$ is defined as follows:

$$\mathcal{L}_{\text{PT}}(\theta; \mathcal{D}_{\text{PT}}) = -\mathbb{E}_{(\mathbf{x}, x_N) \sim \mathcal{D}_{\text{PT}}} [\log p_{\theta}(x_N | \mathbf{x})],$$

where $\mathbf{x} = (x_0, \dots, x_{N-1})$ and $N \in \mathbb{N}$, such that (x_0, \dots, x_N) forms a prefix in some piece of pre-training text. \mathcal{D}_{PT} stands for pre-training dataset.

Supervised Fine-tuning (SFT). SFT adjusts the pre-trained models to follow specific instructions, utilizing a smaller dataset compared to the pre-training corpus to ensure model alignment with target tasks. For $\mathcal{D}_{\text{SFT}} = \{(\mathbf{x}^i, \mathbf{y}^i)\}_{i=1}^N$ sampled from a high-quality distribution, SFT aims to minimize the negative log-likelihood loss:

$$\mathcal{L}_{\text{SFT}}(\theta; \mathcal{D}_{\text{SFT}}) = -\mathbb{E}_{(\mathbf{x}, \mathbf{y}) \sim \mathcal{D}_{\text{SFT}}} [\log p_{\theta}(\mathbf{y} | \mathbf{x})].$$

Given that $\mathbb{E}_{(\mathbf{x}, \mathbf{y}) \sim \mathcal{D}_{\text{SFT}}} [\log p_{\mathcal{D}}(\mathbf{y} | \mathbf{x})]$ is fixed when specifying \mathcal{D}_{SFT} , the optimization objective \mathcal{L}_{SFT} becomes the Kullback-Leibler (KL) divergence between p_{θ} and the SFT distribution.

Lossless Compression. The goal of lossless compression is to find a compression protocol that encodes a given dataset \mathcal{D} and its distribution $\mathcal{P}_{\mathcal{D}}$ with the smallest possible expected length and allows for a decoding scheme that can perfectly reconstruct the original dataset. According to Shannon’s source coding theorem (Shannon, 1948), for a random variable follows $\mathcal{P}_{\mathcal{D}}$, the expected code length \mathcal{L} of any lossless compression protocol satisfies:

$$\mathcal{L} \geq H(\mathcal{P}_{\mathcal{D}}),$$

where $H(\mathcal{P}_{\mathcal{D}})$ is the Shannon entropy of $\mathcal{P}_{\mathcal{D}}$.

Compression and Prediction. Compression and prediction are tightly interconnected. Consider a model p_{θ} and $\mathbf{x} = (x_0, \dots, x_{m-1})$ derived from a dataset \mathcal{D} , the expected code length \mathcal{L} under arithmetic coding (Witten et al., 1987) satisfies:

$$\mathcal{L} = \mathbb{E}_{\mathbf{x} \sim \mathcal{D}} \left[\sum_{0 \leq k \leq m} -\log_2 p_{\theta}(x_k | x_0, \dots, x_{k-1}) \right],$$

which is the current training objective of language models. Minimizing log-likelihood loss is equivalent to minimizing the compression rate when models act as a lossless compressor. Thus, optimal compression and prediction are equivalent (Delétang et al., 2023; Hutter, 2005). Experiments show the equivalence between large language model prediction and compression (Delétang et al., 2023), and that compression performance correlates linearly with intelligence (Huang et al., 2024).

2.2 The Compression Protocol of LLMs

We aim to study the dynamic changes in language models during training and alignment. Given the equivalence between language model training and data compression (Delétang et al., 2023), a feasible modeling approach is to treat the language model as a lossless compression protocol. The process of training and aligning the model on different datasets can be equivalently viewed as the joint compression of these datasets by the protocol. The model’s compression rate on various datasets serves as a surrogate metric for the loss during training and alignment. In this section, we detail the modeling specifics of this compression protocol.

Considering the impact of tokenization on compression rate, we use tokenized sequences as input and output modalities. To simplify the model’s vocabulary representation, we assume that the tokenized vocabulary contains only binary tokens.

Assumption 2.1 (Binary Tokens). In the tokenization process applied to the datasets, without loss of generality, we assume the token table contains only binary tokens (specifically 0/1) and is uniform across all datasets.

After the tokenization process, all responses in the dataset are sequential combinations of symbols from the alphabet. Therefore, all possible responses in the dataset can naturally be modeled using a tree, with the node weights representing the occurrence probabilities of the corresponding answers or answer prefixes in the dataset. This leads us to define the token tree for the dataset.

Definition 2.2 (Token Tree \mathcal{T}). For a dataset $\mathcal{D} = \{z_i \in \{0|1\}^\infty \mid i = 1, 2, \dots\}$, the token tree of \mathcal{D} , denoted as $\mathcal{T}_{\mathcal{D}}$, is defined as follows: each node has child nodes labeled 0 or 1, along with an end-of-sequence (EOS) leaf node. The path from the root to a leaf node defines each response z_i , with the corresponding EOS node weight representing the response’s probability while the weight of non-leaf nodes is the sum of the weights of their child nodes.

Under the token tree modeling of the dataset, the training process of the model can be viewed as learning the node weights of the token tree. However, due to the finite size of the model’s parameters in real-world scenarios, the model cannot perfectly capture the node weights at arbitrary depths of the token tree. As a result, we assume that the model’s parameter size is monotone with the depth of the token tree it can model.

Assumption 2.3 (Scale of \mathcal{T} is Monotone with Model Size). Consider a parameterized model $p_\theta(\cdot)$ and a dataset \mathcal{D} . We assume that the depth of the portion of $\mathcal{T}_{\mathcal{D}}$ that can be perfectly modelled by p_θ is monotonically increasing with the size of θ .

Based on the above assumptions, we can define the compression protocol followed during the model training and alignment process.

Definition 2.4 (The Compression Protocol). Consider using the model $p_\theta(\cdot)$ to compress the dataset \mathcal{D} . The compression protocol is defined in two steps: a) Prune the token tree of \mathcal{D} , retaining only the top d layers. b) Apply Huffman coding (Huffman, 1952) to compress the pruned token tree. Specifically, each response from the root node to a leaf node is treated as a symbol in the Huffman coding alphabet, and the weight of the leaf node is the probability of the symbol.

Due to the optimality and losslessness of Huffman coding (Huffman, 1952), the compression protocol ensures optimal compression while preserving losslessness. Based on the compression protocol, we can calculate the model’s ideal coding length and other information-theoretic metrics.

Theorem 2.5 (Ideal Code Length). Consider a finite parameter model $p_{\theta}(\cdot)$ training on dataset \mathcal{D} , the ideal code length $\mathcal{L}_{p_{\theta}}(\mathbf{x})$ of a random response \mathbf{x} compressed by p_{θ} can be expressed as:

$$\mathbb{E}[\mathcal{L}_{p_{\theta}}(\mathbf{x})] = \left\lceil \frac{|\mathbf{x}|}{d} \right\rceil \left[- \sum_{l=1}^d \sum_{j=1}^{2^{l-1}} p_{lj} \log p_{lj} \right]$$

where d represents the depth of the $\mathcal{T}_{\mathcal{D}}$ after pruning under Definition 2.4 protocol, and p_{lj} represents the probability values of the leaf nodes for the j -th node at the l -th layer.

Since training and alignment often involve multiple datasets with different and independent distributions, we need to consider the joint compression scenario for multiple datasets. For N pairwise disjoint datasets $\mathcal{D}_1, \dots, \mathcal{D}_N$, the node weights $p_{lj}^{\mathcal{D}}$ of the token tree for the combined dataset $\mathcal{D} = \bigcup_{i=1}^N \mathcal{D}_i$ satisfy:

$$p_{lj}^{\mathcal{D}} = \frac{\sum_{i=1}^N p_{lj}^{\mathcal{D}_i} |\mathcal{D}_i|}{\sum_{i=1}^N |\mathcal{D}_i|},$$

where $p_{lj}^{\mathcal{D}_i}$ stands for the probability value for nodes in $\mathcal{T}_{\mathcal{D}_i}$ while $|\mathcal{D}_i|$ represents the size of \mathcal{D}_i . Thus, the compression rate $\gamma_{p_{\theta}}^{\mathcal{D}_i}$ on specific datasets can also be defined accordingly:

$$\begin{aligned} \gamma_{p_{\theta}}^{\mathcal{D}_i} &= \mathbb{E}_{\mathbf{x} \sim \mathcal{P}_i} \left[\frac{\mathbb{E}_{\mathbf{x} \sim \mathcal{P}_i} [\mathcal{L}_{p_{\theta}}^{\mathcal{D}_i}(\mathbf{x})]}{|\mathbf{x}|} \right] \\ &= \Theta \left(- \frac{\sum_{l=1}^d \sum_{j=1}^{2^{l-1}} p_{lj}^{\mathcal{D}_i} \log p_{lj}^{\mathcal{D}_i}}{d} \right). \end{aligned}$$

Here, the compression rate is defined as the compressed encoding length divided by the original length (Delétang et al., 2023) and ensures consistency between the training and compression objective, which means that minimizing the training loss is equivalent to minimizing the compression rate.

2.3 The Formal Definition of Elasticity

To formalize *inverse alignment* and *elasticity*, we provide precise definitions of these concepts.

Definition 2.6 (Inverse Alignment). Given an initial language model p_{θ_0} , for any ϵ , after aligning it on dataset \mathcal{D}_a to obtain the aligned model p_{θ_1} , we use dataset \mathcal{D}_b (where $|\mathcal{D}_b| \ll |\mathcal{D}_a|$) to perform an operation on p_{θ_1} . This process yields an *inverse-aligned model* $p_{\theta'_0}$, such that $\rho(p_{\theta'_0}, p_{\theta_0}) \leq \epsilon$ for a given metric function ρ (which can be viewed as a measure of behavioral and distributional proximity between two models). We define the transition from p_{θ_1} back to p_{θ_0} as *inverse alignment*.

Definition 2.7 (The Elasticity of LLMs). Consider a language model p_{θ_0} and transformation $p_{\theta_0} \xrightarrow{f(\mathcal{D}_a)} p_{\theta_1}$, *elasticity* is said to exist in $(p_{\theta_0}, \mathcal{D}_a)$ if there is an algorithmically simple *inverse operation* g and a dataset \mathcal{D}_b such that $|\mathcal{D}_b| \ll |\mathcal{D}_a|$, with the property that:

$$p_{\theta_1} \xrightarrow{g(\mathcal{D}_b)} p_{\theta'_0} \text{ and } \rho(p_{\theta'_0}, p_{\theta_0}) \leq \epsilon_0.$$

where ϵ_0 is a constant.

In the context of the compression theorem, we use compression rate $\gamma_{p_{\theta}}^{\mathcal{D}_i}$ as the metric function ρ to evaluate *elasticity* during the alignment process.

3 Why Elasticity Affects Alignment?

By now, we hope to have convinced the reader of the concept of compression modeling in language models' training and alignment. In the following, we apply this to analyze language models' training and alignment process, focusing on the underlying reasons that lead the model to alignment resistance.

In Figure 1, we have already presented the theorem of *elasticity*: when subject to fine-tuning perturbations, language models tend to retain the distribution associated with larger datasets while rejecting that of smaller ones. But why *elasticity* resists alignment? Is there a corresponding *elastic invariant*? How does *elasticity* make *inverse alignment* possible? In this section, we will formalize *elasticity* of language models and analyze the impact of *elasticity* on the model's behavior.

3.1 Formal Derivation of Elasticity

Our primary goal is to investigate the behavioral changes of a language model after pre-training and alignment, particularly in response to perturbations, typically caused by fine-tuning with a minimal

dataset. We use compression rate as an evaluation metric to assess these changes. In analyzing the model’s behavior, we focus on two datasets: \mathcal{D}_1 , a larger dataset representing pre-training or the primary objective of alignment, and \mathcal{D}_2 , a smaller dataset representing alignment process or the secondary objectives of alignment. Without loss of generality, we assume that the distributions of these datasets are distinct and independent.

Due to the different scales of compression rates obtained for different datasets by the model, we consider normalizing the compression rates for different datasets.

Definition 3.1 (Normalized Compression Rate). For N pairwise disjoint datasets $\mathcal{D}_1, \dots, \mathcal{D}_N$ and a parameter model p_θ compressing $\mathcal{D} = \bigcup_{i=1}^N \mathcal{D}_i$, the normalized compression rate $\gamma_{p_\theta}^{\mathcal{D}_i/\mathcal{D}}$ for a particular dataset \mathcal{D}_i is defined as:

$$\gamma_{p_\theta}^{\mathcal{D}_i/\mathcal{D}} = \log M - \gamma_{p_\theta}^{\mathcal{D}_i}, \quad (1)$$

where M is the number of leaf nodes of the pruned tree \mathcal{T}'_i of dataset \mathcal{D}_i .

The definition of normalized compression rate allows comparing the model’s compression performance across different datasets. The smaller the normalized compression rate of a dataset, the better the model’s compression performance on the dataset.

With this definition in hand, we proceed to our main result: language models exhibit *elasticity*.

Theorem 3.2 (*Elasticity of Language Models*). Consider datasets $\mathcal{D}_1, \mathcal{D}_2$ and perturbation \mathcal{D}_3 each with a Pareto mass distribution (Newman, 2005), and the model $p_\theta(\cdot)$ trained on $\mathcal{D} = \mathcal{D}_1 \cup \mathcal{D}_2 \cup \mathcal{D}_3$. When dataset \mathcal{D}_3 ’s data volume $|\mathcal{D}_3|$ changes, the normalized compression rates $\gamma_{p_\theta}^{\mathcal{D}_1/\mathcal{D}}$ and $\gamma_{p_\theta}^{\mathcal{D}_2/\mathcal{D}}$ satisfies:

$$\frac{d\gamma_{p_\theta}^{\mathcal{D}_2/\mathcal{D}}}{dl} = \Theta \left(k \frac{d\gamma_{p_\theta}^{\mathcal{D}_1/\mathcal{D}}}{dl} \right), \quad (2)$$

$$\frac{d\gamma_{p_\theta}^{\mathcal{D}_1/\mathcal{D}}}{dl} > 0, \frac{d\gamma_{p_\theta}^{\mathcal{D}_2/\mathcal{D}}}{dl} > 0,$$

where $l = \frac{|\mathcal{D}_3|}{|\mathcal{D}_2|} \ll 1$, $k = \frac{|\mathcal{D}_1|}{|\mathcal{D}_2|} \gg 1$.

Theorem 3.2 shows that as the perturbation increases, the normalized compression rates of the model for both datasets \mathcal{D}_1 and \mathcal{D}_2 increase and the rate of increase is strongly correlated with the size

of the datasets. Unlike the proportional increase in compression rates across different datasets, the language model seems to *prefer* the dataset with a larger volume, leading to biased model behavior after the perturbation.

3.2 Elasticity and Inverse Alignment

Theorem 3.2 shows the normalized compression rate change of different datasets is inversely proportional to their sizes under perturbations. A significant size difference between the pre-training and alignment datasets causes rapid performance degradation on the alignment dataset due to the inverse relationship, often spanning several orders of magnitude.

Intuitively, the model’s compression process across multiple datasets is akin to resource allocation between towns: in a region with both a large metropolis and rural villages, to maximize overall economic productivity, resources are typically allocated to the metropolis first, to leverage its scale and agglomeration effects. In other words, the metropolis/large dataset occupies a dominant position in the system.

Therefore, the *elasticity* of language models makes *inverse alignment* possible. Due to the substantial data volume disparity between pre-training and alignment datasets, the model tends to revert to the pre-training rather than alignment distribution when subsequent perturbations occur. This indicates an inherent tendency toward *inverse alignment* during fine-tuning. Maximizing the impact of *elasticity* through well-designed perturbations will be key to achieving true *inverse alignment*.

3.3 Elasticity and the Hooke’s Law.

The inverse proportionality result in Theorem 3.2 provides a potential invariant in the model training and alignment process: after perturbation, the rate of change in the compression rates of different datasets is inversely proportional to their sizes, with the product being a constant. This constant characterizes the impact of the perturbation on the model and indirectly describes the model’s resistance to perturbations, or its *elasticity*.

The *elasticity* of the model can be intuitively analogized to a series system of springs, as shown in Figure 1. Consider two massless springs in series, with spring constants k_1 and k_2 , respectively. When the entire system undergoes deformation due to an external force F , the system reaches a stable state, and the elastic force exerted by each spring

is equal to F . According to Hooke’s Law (Hooke, 2016), the elongation Δl_1 and Δl_2 of each spring is inversely proportional to its spring constant. Thus, in this system, we have:

$$F \propto k_1 \cdot \Delta l_1 = k_2 \cdot \Delta l_2 .$$

In the language model setting, after integrating Theorem 3.2 to l , we obtain $\Delta \gamma_{p\theta}^{\mathcal{D}_i/\mathcal{D}}$ across different datasets, which is equivalent to the change in the KL divergence $\Delta D_{\text{KL}}(\mathcal{P}_{p\theta} \parallel \mathcal{P}_{\mathcal{D}_i})$ between the model’s distribution and the distributions of the individual datasets, is inversely proportional to the size of the datasets $|\mathcal{D}_i|$. Analogous to the series spring model, the *elasticity* F in LLMs satisfies:

$$F \propto |\mathcal{D}_i| \cdot \Delta D_{\text{KL}}(\mathcal{P}_{p\theta} \parallel \mathcal{P}_{\mathcal{D}_i}) , \quad (3)$$

where ΔD_{KL} corresponds to Δl in the spring model, while $|\mathcal{D}|$ corresponds to the spring constant k , thus leading to the *elasticity* of LLMs.

4 How Elasticity Resists Alignment?

In the previous sections, we proved that LLMs have *elasticity*. This section will analyze two specific phenomena of it:

- **Resistance for Pre-Trained Models.** Models tend to maintain the original distribution and resist alignment;
- **Rebound for Post-Trained Models.** Fine-tuning in the opposite direction of post-training (e.g., safe vs. unsafe) causes post-trained models to return quickly to the pre-training distribution.

4.1 Existence of Resistance

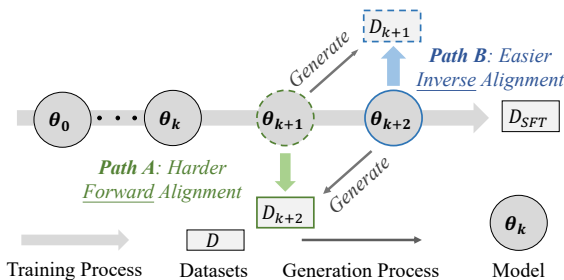


Figure 2: **Experiment pipeline for validating resistance.** We conceptualize *resistance* as: *inverse alignment* is easier than *forward alignment*.

Experiment Design. We verify the existence of *resistance* by arguing that *forward alignment* is harder than *inverse alignment* for pre-trained models. Specifically, we first perform one epoch of SFT on a pre-trained LLM with parameters θ_0 , saving the slices $\{\theta_1, \theta_2, \dots, \theta_n\}$. Subsequently, without loss of generality, we collect the responses of slices θ_{k+1} and θ_{k+2} on hold-out prompts, forming datasets D_{k+1} and D_{k+2} . As shown in Figure 2, we define *forward alignment (Path A)* as the process of training θ_{k+1} on D_{k+2} , and *inverse alignment (Path B)* as the process of training θ_{k+2} on D_{k+1} .

Experiment Setup. We select different SFT datasets including Alpaca (Taori et al., 2023), TruthfulQA (Lin et al., 2022), and Beavertails (Ji et al., 2024). We divide them into three equal parts to obtain three corresponding slices $\{\theta_1, \theta_2, \theta_3\}$. We consider Llama2-7B, Llama2-13B, and Llama3-8B (Touvron et al., 2023) as the base model θ_0 .

Experiment Results. As shown in Table 1, the experimental results show that the *inverse alignment* training loss is smaller than the *forward alignment* ones. These results hold across all models and datasets. We also compare θ_1 with θ_3 , and the results are also as expected. All experimental results demonstrate that *inverse alignment* is easier than *forward alignment* across diverse models and datasets and validate the existence of *resistance*.

4.2 Existence of Rebound

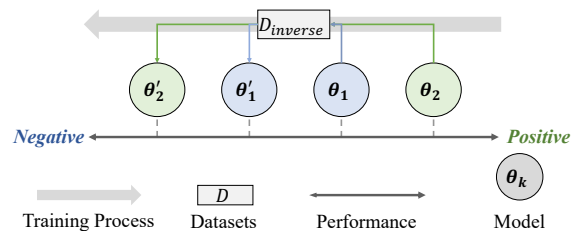


Figure 3: **Experiment pipeline for validating rebound.** We conceptualize *rebound* as: the more **positive** the post-trained models’ performance, the more **negative** it becomes after inverse finetuning.

Experiment Design. We verify the existence of *rebound* by arguing that for post-trained models, the more **positive** the post-trained models’ performance, the more **negative** it becomes after *inverse alignment*. We validate tasks involving two opposing characteristics (e.g. safe and unsafe). We first train slices $\{\theta_1, \theta_2, \dots, \theta_n\}$ based on a pre-trained model θ_0 using positive (e.g., safe) data of various

Datasets	Base Models	$\theta_2 \rightarrow \theta_1$ vs. $\theta_1 \rightarrow \theta_2$	$\theta_3 \rightarrow \theta_2$ vs. $\theta_2 \rightarrow \theta_3$	$\theta_3 \rightarrow \theta_1$ vs. $\theta_1 \rightarrow \theta_3$
Alpaca	Llama2-7B	0.1589 ↓ 0.2018 ↑	0.1953 ↓ 0.2143 ↑	0.1666 ↓ 0.2346 ↑
	Llama2-13B	0.1772 ↓ 0.1958 ↑	0.2149 ↓ 0.2408 ↑	0.1835 ↓ 0.2345 ↑
	Llama3-8B	0.2540 ↓ 0.2573 ↑	0.2268 ↓ 0.3229 ↑	0.2341 ↓ 0.2589 ↑
Truthful	Llama2-7B	0.1909 ↓ 0.2069 ↑	0.1719 ↓ 0.1721 ↑	0.2011 ↓ 0.2542 ↑
	Llama2-13B	0.1704 ↓ 0.1830 ↑	0.1544 ↓ 0.1640 ↑	0.1825 ↓ 0.2429 ↑
	Llama3-8B	0.2118 ↓ 0.2256 ↑	0.2100 ↓ 0.2173 ↑	0.2393 ↓ 0.2898 ↑
Safe	Llama2-7B	0.2730 ↓ 0.2809 ↑	0.2654 ↓ 0.2691 ↑	0.2845 ↓ 0.2883 ↑
	Llama2-13B	0.2419 ↓ 0.2439 ↑	0.2320 ↓ 0.2327 ↑	0.2464 ↓ 0.2606 ↑
	Llama3-8B	0.2097 ↓ 0.2156 ↑	0.2008 ↓ 0.2427 ↑	0.2277 ↓ 0.2709 ↑

Table 1: Comparison between *inverse alignment* and *forward alignment* training loss. Under different model, task, and stage slicing settings, *forward alignment* is more challenging than *inverse alignment*, i.e., the loss is higher. This indicates that pre-trained models tend to maintain their original distribution.

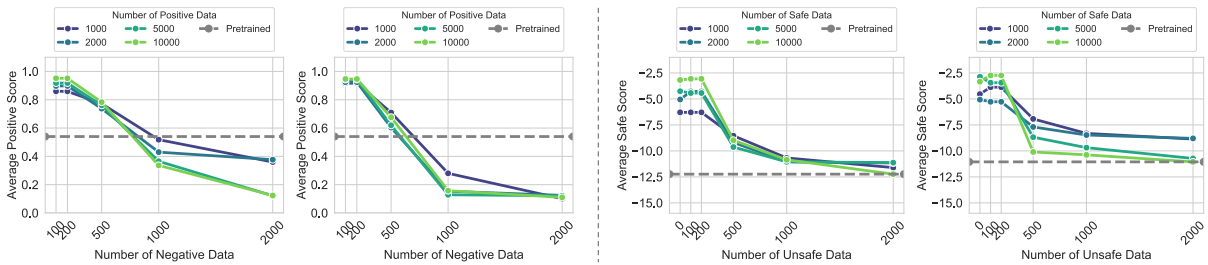


Figure 4: Experimental results for validating the existence of *rebound* (left: IMDb, right: Beavertails). The left part of each sub-figure is the performance of Gemma-2B (Team et al., 2024) while the right is Llama2-7B (Touvron et al., 2023), respectively. Models trained with more positive data initially perform better, but perform worse after fine-tuning with negative data.

volumes. Then we perform inverse finetuning on these slices using negative data (i.e., unsafe).

Tasks and Datasets. We select two tasks: positive generation and single-turn safe conversation. For the former, we use the data classified as positive or negative in the IMDb dataset (Maas et al., 2011). Referring to (Rafailov et al., 2024), we use the first 2-8 tokens of each complete text as a prompt for LLMs to generate the subsequent content. For the latter, we use the data classified as safe and unsafe in Beavertails (Ji et al., 2024). We organized the positive sample sizes into {1000, 2000, 5000, 10000}, while the negative sample sizes, were divided into {100, 200, 500, 1000, 2000}.

Evaluation and Metrics. We collect the model’s responses on the reserved test prompts. Then we use score models provided by existing research to complete the performance evaluation. For positive style generation, we refer to (Rafailov et al., 2024) and use the Sentiment Roberta model (Hartmann et al., 2023) to classify the responses, taking the proportion of all responses classified as positive as the model score. For single-turn safe dialogue, we use the cost model (Dai et al., 2024) to score the

safety of each response, using the average score of all responses as the model score.

Results. We evaluate the *rebound* phenomenon on Llama2-7B (Touvron et al., 2023) and Gemma-2B (Team et al., 2024). The experimental results in Figure 4 show that, for models fine-tuned with a larger amount of positive sample data, their performance drops quicker under only a small amount of negative sample fine-tuning. Subsequently, the performance decline slows down and tends to stabilize. This result also confirms the previous conclusion: the initial rapid decline is due to *rebound*, as the model is far from the pre-trained distribution; while the later stabilization of the countermeasure is due to *resistance*, as the model is already close to the pre-trained distribution.

4.3 Internal Factor of *Rebound*

We conduct an in-depth analysis of the internal factors affecting the *rebound* phenomenon since it is crucial for the robustness of LLMs alignment.

***Rebound* Increases with Model Size.** To examine how *rebound* changes with model size, we conducted experiments on Qwen models (Bai et al.,

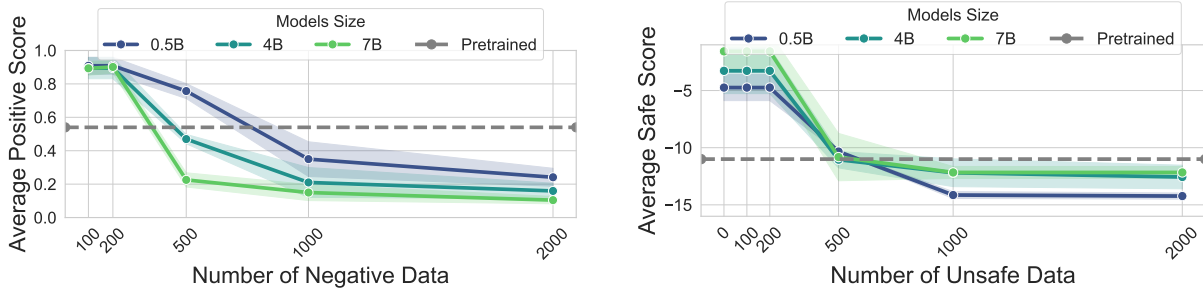


Figure 5: **Experimental results for validating *rebound* increases with model size (left: IMDb, right: Beavertails).** All single line covers positive data volume settings as Figure 4, with shadow denoting std.

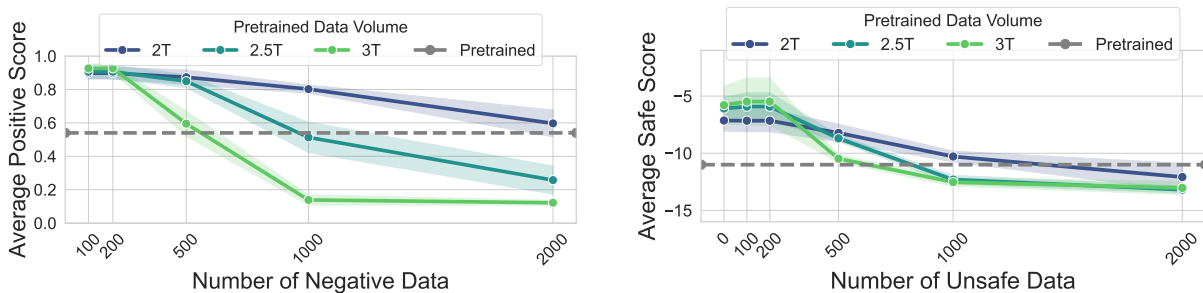


Figure 6: **Experimental Results for Validating *Rebound* increases with pre-training data Volume. (left: IMDb, right: Beavertails).** All single line covers positive data volume settings as Figure 4, with shadow denoting std.

2023) with 0.5B, 4B, and 7B parameters. In Figure 5, as the model parameter size increases, the initial performance decline due to negative data fine-tuning is faster, while the subsequent decline is slower. This indicates that as the parameter size increases, there is an increased *rebound* in response to both positive and negative data.

***Rebound* Increases with Pre-training Data Volume.** To verify that *rebound* increases with the growth of pre-training data, we vary pre-training slices (2.0T, 2.5T, and 3.0T) released by TinyLlama (Zhang et al., 2024a) and conduct the same experiment. As shown in Figure 6, when the pre-training data volume increases, the initial performance decline due to negative data fine-tuning is faster, while the subsequent decline is slower. It demonstrates that larger pre-training data volumes reinforce the *rebound* of LLMs.

5 Conclusion and Outlook

Our work uncovers a possible mechanism underlying the fragility of alignment: the *elasticity* of language models. We demonstrate that upon perturbation, the normalized compression rate of language models changes inversely with dataset size, making them more inclined to retain pre-training distributions while forgetting alignment distribu-

tions, thus resisting alignment. Through extensive experiments, we validate the universality of this *elasticity* effect, observing that it strengthens as model size and pre-training data scale up. Fundamentally, our findings support a core assertion: language models exhibit *elasticity*, inherently resisting alignment.

5.1 Limitations

Theory-wise, the primary limitation of our work is our specification of the *mass distribution* (Assumption B.6), and empirical studies on the exact form of this distribution shall be valuable. Experiment-wise, we have not systematically validated *elasticity* throughout the entire lifecycle of pre-training and alignment phases due to cost constraints. In future works, we plan to focus on whether this phenomenon is universally applicable, such as in multimodal models. Additionally, we aim to theoretically uncover the relationship between model *elasticity* and *scaling laws*, specifically determining the amount of training data required for *elasticity* to manifest and quantitatively analyzing whether *elasticity* intensifies as model parameters increase.

5.2 Broader Impacts

Rethinking Fine-tuning. Alignment fine-tuning methods aim to efficiently modify the distribution

of LLMs with minimal data to enhance their safety mechanisms. From the perspective of model *elasticity*, we require more robust alignment methods to ensure that modifications to model parameters extend beyond superficial changes (Qi et al., 2024a), preventing the emergence of more effective *inverse alignment* methods. Data cleansing during pre-training is an effective strategy to enhance the malleability of the model’s final distribution (He et al., 2024; Qi et al., 2024b), although this approach is not cost-effective. We anticipate that future work, grounded in the *elasticity* of the language model, will design more robust alignment algorithms (Revel et al., 2024; Zhang et al., 2024b; Chen et al., 2024; Sheshadri et al., 2024; Liu et al., 2024), enabling true alignment of LLMs.

Rethinking Open-sourcing. Open-sourcing is a double-edged sword (Seger et al., 2023; Anwar et al., 2024; Kukreja et al., 2024). While making models publicly available enables the technical community to test and address potential vulnerabilities rapidly, it simultaneously increases the risk of model misuse (Urbina et al., 2022; Sandbrink, 2023; Reuel et al., 2024). From the *inverse alignment’s* perspective, if advanced *inverse alignment’s* methods become feasible, the cost of jail-breaking aligned models will plummet, disrupting the offence-defence balance in the open-source process (Shapiro and Siegel, 2010). We hope insights into *elasticity* will drive the development of robust alignment algorithms, enabling models to maintain safety throughout their lifecycle (Madiaga, 2021).

References

- Josh Achiam, Steven Adler, Sandhini Agarwal, Lama Ahmad, Ilge Akkaya, Florencia Leoni Aleman, Diogo Almeida, Janko Altenschmidt, Sam Altman, Shyamal Anadkat, et al. 2023. Gpt-4 technical report. *arXiv preprint arXiv:2303.08774*.
- Usman Anwar, Abulhair Saparov, Javier Rando, Daniel Paleka, Miles Turpin, Peter Hase, Ekdeep Singh Lubana, Erik Jenner, Stephen Casper, Oliver Sourbut, et al. 2024. Foundational challenges in assuring alignment and safety of large language models. *arXiv preprint arXiv:2404.09932*.
- Jinze Bai, Shuai Bai, Yunfei Chu, Zeyu Cui, Kai Dang, Xiaodong Deng, Yang Fan, Wenbin Ge, Yu Han, Fei Huang, et al. 2023. Qwen technical report. *arXiv preprint arXiv:2309.16609*.
- Yuntao Bai, Andy Jones, Kamal Ndousse, Amanda Askell, Anna Chen, Nova DasSarma, Dawn Drain, Stanislav Fort, Deep Ganguli, Tom Henighan, et al. 2022a. Training a helpful and harmless assistant with reinforcement learning from human feedback. *arXiv preprint arXiv:2204.05862*.
- Yuntao Bai, Saurav Kadavath, Sandipan Kundu, Amanda Askell, Jackson Kernion, Andy Jones, Anna Chen, Anna Goldie, Azalia Mirhoseini, Cameron McKinnon, et al. 2022b. Constitutional ai: Harmlessness from ai feedback. *arXiv preprint arXiv:2212.08073*.
- Stephen Casper, Xander Davies, Claudia Shi, Thomas Krendl Gilbert, Jérémy Scheurer, Javier Rando, Rachel Freedman, Tomasz Korbak, David Lindner, Pedro Freire, Tony Tong Wang, Samuel Marks, Charbel-Raphael Segerie, Micah Carroll, Andi Peng, Phillip Christoffersen, Mehul Damani, Stewart Slocum, Usman Anwar, Anand Siththaranjan, Max Nadeau, Eric J Michaud, Jacob Pfau, Dmitrii Krashennnikov, Xin Chen, Lauro Langosco, Peter Hase, Erdem Biyik, Anca Dragan, David Krueger, Dorsa Sadigh, and Dylan Hadfield-Menell. 2023. Open problems and fundamental limitations of reinforcement learning from human feedback. *Transactions on Machine Learning Research*. Survey Certification.
- Yingfa Chen, Zhengyan Zhang, Xu Han, Chaojun Xiao, Zhiyuan Liu, Chen Chen, Kuai Li, Tao Yang, and Maosong Sun. 2024. Robust and scalable model editing for large language models. *arXiv preprint arXiv:2403.17431*.
- Michael K Cohen, Marcus Hutter, Yoshua Bengio, and Stuart Russell. 2024. RL, but don’t do anything i wouldn’t do. *arXiv preprint arXiv:2410.06213*.
- Ganqu Cui, Lifan Yuan, Ning Ding, Guanming Yao, Bingxiang He, Wei Zhu, Yuan Ni, Guotong Xie, Ruobing Xie, Yankai Lin, et al. 2024. Ultrafeedback: Boosting language models with scaled ai feedback. In *Forty-first International Conference on Machine Learning*.
- Josef Dai, Xuehai Pan, Ruiyang Sun, Jiaming Ji, Xinbo Xu, Mickel Liu, Yizhou Wang, and Yaodong Yang. 2024. Safe rlhf: Safe reinforcement learning from human feedback. In *The Twelfth International Conference on Learning Representations*.
- Grégoire Delétang, Anian Ruoss, Paul-Ambroise Duquenne, Elliot Catt, Tim Genewein, Christopher Mattern, Jordi Grau-Moya, Li Kevin Wenliang, Matthew Aitchison, Laurent Orseau, et al. 2023. Language modeling is compression. *arXiv preprint arXiv:2309.10668*.
- Hanze Dong, Wei Xiong, Deepanshu Goyal, Yihan Zhang, Winnie Chow, Rui Pan, Shizhe Diao, Jipeng Zhang, SHUM KaShun, and Tong Zhang. 2023. Raft: Reward ranked finetuning for generative foundation model alignment. *Transactions on Machine Learning Research*.

- Zhichen Dong, Zhanhui Zhou, Chao Yang, Jing Shao, and Yu Qiao. 2024. Attacks, defenses and evaluations for llm conversation safety: A survey. *arXiv preprint arXiv:2402.09283*.
- Caglar Gulcehre, Tom Le Paine, Srivatsan Srinivasan, Ksenia Konyushkova, Lotte Weerts, Abhishek Sharma, Aditya Siddhant, Alex Ahern, Miaosen Wang, Chenjie Gu, et al. 2023. Reinforced self-training (rest) for language modeling. *arXiv preprint arXiv:2308.08998*.
- Jochen Hartmann, Mark Heitmann, Christian Siebert, and Christina Schamp. 2023. More than a feeling: Accuracy and application of sentiment analysis. *International Journal of Research in Marketing*, 40(1):75–87.
- Luxi He, Mengzhou Xia, and Peter Henderson. 2024. What’s in your " safe " data?: Identifying benign data that breaks safety. *arXiv preprint arXiv:2404.01099*.
- Robert Hooke. 2016. *Lectures de potentia restitutiva, or of spring explaining the power of springing bodies*. 6. John Martyn.
- Yuzhen Huang, Jinghan Zhang, Zifei Shan, and Junxian He. 2024. Compression represents intelligence linearly. *arXiv preprint arXiv:2404.09937*.
- Evan Hubinger, Carson Denison, Jesse Mu, Mike Lambert, Meg Tong, Monte MacDiarmid, Tamera Latham, Daniel M Ziegler, Tim Maxwell, Newton Cheng, et al. 2024. Sleeper agents: Training deceptive llms that persist through safety training. *arXiv preprint arXiv:2401.05566*.
- David A Huffman. 1952. A method for the construction of minimum-redundancy codes. *Proceedings of the IRE*, 40(9):1098–1101.
- Marcus Hutter. 2005. *Universal Artificial Intelligence: Sequential Decisions Based On Algorithmic Probability*. Springer Science & Business Media.
- Samyak Jain, Robert Kirk, Ekdeep Singh Lubana, Robert P Dick, Hidenori Tanaka, Edward Grefenstette, Tim Rocktäschel, and David Scott Krueger. 2023. Mechanistically analyzing the effects of fine-tuning on procedurally defined tasks. *arXiv preprint arXiv:2311.12786*.
- Jiaming Ji, Mickel Liu, Josef Dai, Xuehai Pan, Chi Zhang, Ce Bian, Boyuan Chen, Ruiyang Sun, Yizhou Wang, and Yaodong Yang. 2024. Beavertails: Towards improved safety alignment of llm via a human-preference dataset. *Advances in Neural Information Processing Systems*, 36.
- Jiaming Ji, Tianyi Qiu, Boyuan Chen, Borong Zhang, Hantao Lou, Kaile Wang, Yawen Duan, Zhonghao He, Jiayi Zhou, Zhaowei Zhang, et al. 2023. Ai alignment: A comprehensive survey. *arXiv preprint arXiv:2310.19852*.
- Sanjay Kukreja, Tarun Kumar, Amit Purohit, Abhijit Dasgupta, and Debashis Guha. 2024. A literature survey on open source large language models. In *Proceedings of the 2024 7th International Conference on Computers in Management and Business*, pages 133–143.
- Harrison Lee, Samrat Phatale, Hassan Mansoor, Kellie Lu, Thomas Mesnard, Colton Bishop, Victor Carbone, and Abhinav Rastogi. 2023. Rlaif: Scaling reinforcement learning from human feedback with ai feedback. *arXiv preprint arXiv:2309.00267*.
- Ziniu Li, Tian Xu, Yushun Zhang, Yang Yu, Ruoyu Sun, and Zhi-Quan Luo. 2023. Remax: A simple, effective, and efficient method for aligning large language models. *arXiv preprint arXiv:2310.10505*.
- Stephanie Lin, Jacob Hilton, and Owain Evans. 2022. Truthfulqa: Measuring how models mimic human falsehoods. In *Proceedings of the 60th Annual Meeting of the Association for Computational Linguistics (Volume 1: Long Papers)*, pages 3214–3252.
- Tianqi Liu, Wei Xiong, Jie Ren, Lichang Chen, Junru Wu, Rishabh Joshi, Yang Gao, Jiaming Shen, Zhen Qin, Tianhe Yu, et al. 2024. Rrm: Robust reward model training mitigates reward hacking. *arXiv preprint arXiv:2409.13156*.
- Andrew Maas, Raymond E Daly, Peter T Pham, Dan Huang, Andrew Y Ng, and Christopher Potts. 2011. Learning word vectors for sentiment analysis. In *Proceedings of the 49th annual meeting of the association for computational linguistics: Human language technologies*, pages 142–150.
- Tambiama Madiaga. 2021. Artificial intelligence act. *European Parliament: European Parliamentary Research Service*.
- Chris Mingard, Guillermo Valle-Pérez, Joar Skalse, and Ard A Louis. 2021. Is sgd a bayesian sampler? well, almost. *Journal of Machine Learning Research*, 22(79):1–64.
- Mark EJ Newman. 2005. Power laws, pareto distributions and zipf’s law. *Contemporary physics*, 46(5):323–351.
- Long Ouyang, Jeffrey Wu, Xu Jiang, Diogo Almeida, Carroll Wainwright, Pamela Mishkin, Chong Zhang, Sandhini Agarwal, Katarina Slama, Alex Ray, et al. 2022. Training language models to follow instructions with human feedback. *Advances in neural information processing systems*, 35:27730–27744.
- Xiangyu Qi, Ashwinee Panda, Kaifeng Lyu, Xiao Ma, Subhrajit Roy, Ahmad Beirami, Prateek Mittal, and Peter Henderson. 2024a. Safety alignment should be made more than just a few tokens deep. *arXiv preprint arXiv:2406.05946*.
- Xiangyu Qi, Yi Zeng, Tinghao Xie, Pin-Yu Chen, Ruoxi Jia, Prateek Mittal, and Peter Henderson. 2024b. Fine-tuning aligned language models compromises

- safety, even when users do not intend to! In *The Twelfth International Conference on Learning Representations*.
- Chen Qian, Jie Zhang, Wei Yao, Dongrui Liu, Zhenfei Yin, Yu Qiao, Yong Liu, and Jing Shao. 2024. Towards tracing trustworthiness dynamics: Revisiting pre-training period of large language models. *arXiv preprint arXiv:2402.19465*.
- Rafael Rafailov, Archit Sharma, Eric Mitchell, Christopher D Manning, Stefano Ermon, and Chelsea Finn. 2024. Direct preference optimization: Your language model is secretly a reward model. *Advances in Neural Information Processing Systems*, 36.
- Anka Reuel, Ben Bucknall, Stephen Casper, Tim Fist, Lisa Soder, Onni Aarne, Lewis Hammond, Lujain Ibrahim, Alan Chan, Peter Wills, et al. 2024. Open problems in technical ai governance. *arXiv preprint arXiv:2407.14981*.
- Manon Revel, Matteo Cargnelutti, Tyna Eloundou, and Greg Leppert. 2024. Seal: Systematic error analysis for value alignment. *arXiv preprint arXiv:2408.10270*.
- Jonas B Sandbrink. 2023. Artificial intelligence and biological misuse: Differentiating risks of language models and biological design tools. *arXiv preprint arXiv:2306.13952*.
- Elizabeth Seger, Noemi Dreksler, Richard Moulange, Emily Dardaman, Jonas Schuett, K Wei, Christoph Winter, Mackenzie Arnold, Seán Ó hÉigeartaigh, Anton Korinek, et al. 2023. Open-sourcing highly capable foundation models: An evaluation of risks, benefits, and alternative methods for pursuing open-source objectives. *arXiv preprint arXiv:2311.09227*.
- Claude Elwood Shannon. 1948. A mathematical theory of communication. *The Bell system technical journal*, 27(3):379–423.
- Jacob N Shapiro and David A Siegel. 2010. Is this paper dangerous? balancing secrecy and openness in counterterrorism. *Security Studies*, 19(1):66–98.
- Abhay Sheshadri, Aidan Ewart, Phillip Guo, Aengus Lynch, Cindy Wu, Vivek Hebbar, Henry Sleight, Asa Cooper Stickland, Ethan Perez, Dylan Hadfield-Menell, et al. 2024. Targeted latent adversarial training improves robustness to persistent harmful behaviors in llms. *arXiv e-prints*, pages arXiv–2407.
- Rohan Taori, Ishaan Gulrajani, Tianyi Zhang, Yann Dubois, Xuechen Li, Carlos Guestrin, Percy Liang, and Tatsunori B Hashimoto. 2023. Stanford alpaca: An instruction-following llama model. https://github.com/tatsu-lab/stanford_alpaca.
- Gemma Team, Thomas Mesnard, Cassidy Hardin, Robert Dadashi, Surya Bhupatiraju, Shreya Pathak, Laurent Sifre, Morgane Rivière, Mihir Sanjay Kale, Juliette Love, et al. 2024. Gemma: Open models based on gemini research and technology. *arXiv preprint arXiv:2403.08295*.
- Hugo Touvron, Louis Martin, Kevin Stone, Peter Albert, Amjad Almahairi, Yasmine Babaei, Nikolay Bashlykov, Soumya Batra, Prajjwal Bhargava, Shruti Bhosale, et al. 2023. Llama 2: Open foundation and fine-tuned chat models. *arXiv preprint arXiv:2307.09288*.
- Fabio Urbina, Filippa Lentzos, Cédric Invernizzi, and Sean Ekins. 2022. Dual use of artificial-intelligence-powered drug discovery. *Nature machine intelligence*, 4(3):189–191.
- Boyi Wei, Kaixuan Huang, Yangsibo Huang, Tinghao Xie, Xiangyu Qi, Mengzhou Xia, Prateek Mittal, Mengdi Wang, and Peter Henderson. 2024. Assessing the brittleness of safety alignment via pruning and low-rank modifications. *arXiv preprint arXiv:2402.05162*.
- Jiaxin Wen, Ruiqi Zhong, Akbir Khan, Ethan Perez, Jacob Steinhardt, Minlie Huang, Samuel R Bowman, He He, and Shi Feng. 2024. Language models learn to mislead humans via rlhf. *arXiv preprint arXiv:2409.12822*.
- Ian H Witten, Radford M Neal, and John G Cleary. 1987. Arithmetic coding for data compression. *Communications of the ACM*, 30(6):520–540.
- Wei Xiong, Hanze Dong, Chenlu Ye, Ziqi Wang, Han Zhong, Heng Ji, Nan Jiang, and Tong Zhang. 2024. Iterative preference learning from human feedback: Bridging theory and practice for rlhf under kl-constraint. In *Forty-first International Conference on Machine Learning*.
- Kevin Yang, Dan Klein, Asli Celikyilmaz, Nanyun Peng, and Yuandong Tian. 2023a. Rlcd: Reinforcement learning from contrastive distillation for language model alignment. *arXiv preprint arXiv:2307.12950*.
- Xianjun Yang, Xiao Wang, Qi Zhang, Linda Petzold, William Yang Wang, Xun Zhao, and Dahua Lin. 2023b. Shadow alignment: The ease of subverting safely-aligned language models. *arXiv preprint arXiv:2310.02949*.
- Peiyuan Zhang, Guangtao Zeng, Tianduo Wang, and Wei Lu. 2024a. Tinyllama: An open-source small language model. *arXiv preprint arXiv:2401.02385*.
- Zhexin Zhang, Junxiao Yang, Pei Ke, Shiyao Cui, Chujie Zheng, Hongning Wang, and Minlie Huang. 2024b. Safe unlearning: A surprisingly effective and generalizable solution to defend against jailbreak attacks. *arXiv preprint arXiv:2407.02855*.
- Chunting Zhou, Pengfei Liu, Puxin Xu, Srinivasan Iyer, Jiao Sun, Yuning Mao, Xuezhe Ma, Avia Efrat, Ping Yu, Lili Yu, et al. 2024. Lima: Less is more for alignment. *Advances in Neural Information Processing Systems*, 36.
- George Kingsley Zipf. 1946. The psychology of language. In *Encyclopedia of psychology*, pages 332–341. Philosophical Library.

A Related Work

Pre-trained LLMs often generate offensive content (Casper et al., 2023). Recent initiatives (Ouyang et al., 2022; Bai et al., 2022a) have aimed to align these models to minimize harmful outputs (Bai et al., 2022a; Yang et al., 2023a; Cui et al., 2024). However, studies show that even well-aligned models can be compromised easily, and fine-tuning them on non-malicious datasets might unintentionally impair their safety mechanisms (Yang et al., 2023b; Qi et al., 2024b; Hubinger et al., 2024; Dong et al., 2024). Why is alignment so fragile? Wei et al. (2024) pinpoint areas essential for safety guardrails distinct from utility-relevant regions, achieving this separation at both neuron and rank levels through weight attribution.

B Assumptions and Proofs

Theorem B.1 (Ideal Code Length). *Consider a finite parameter model $p_\theta(\cdot)$ training on dataset \mathcal{D} , the ideal code length $\mathcal{L}_{p_\theta}(\mathbf{x})$ of a random response \mathbf{x} compressed by p_θ can be expressed as follows:*

$$\mathbb{E}[\mathcal{L}_{p_\theta}(\mathbf{x})] = \left\lceil \frac{|\mathbf{x}|}{d} \right\rceil \left[- \sum_{l=1}^d \sum_{j=1}^{2^{l-1}} p_{lj} \log p_{lj} \right],$$

where d represents the depth of the $\mathcal{T}_\mathcal{D}$ after pruning under Definition 2.4 protocol, p_{lj} represents the probability values of the EOS nodes for the j -th node at the l -th layer.

Proof. When $|\mathbf{x}| \leq d$, the compression protocol defined in Definition 2.4 can perfectly compress \mathbf{x} . Hence, the expectation of the ideal code length $\mathcal{L}_{p_\theta}(\mathbf{x})$ satisfies:

$$\mathbb{E}[\mathcal{L}_{p_\theta}(\mathbf{x})] = \left[- \sum_{l=1}^d \sum_{j=1}^{2^{l-1}} p_{lj} \log p_{lj} \right],$$

where d represents the depth of the pruned tree $\mathcal{T}'_\mathcal{D}$ and p_{lj} represents the probability values of the EOS nodes for the j -th node at the l -th layer.

Now consider $sd \leq |\mathbf{x}| \leq (s+1)d$. Let us suppose that $\mathbf{x} = (\mathbf{x}_1 \cdots \mathbf{x}_s \mathbf{x}_{s+1})$, where $|\mathbf{x}_k| = d$, for $k \in \{1, \dots, s\}$ and $|\mathbf{x}_{s+1}| \leq d$. In this case, \mathbf{x} cannot be perfectly compressed by the model. Hence, the compression of \mathbf{x} needs to be performed in segments, and the length of each segment is not greater than d .

$$\begin{aligned} \mathbb{E}_\mathbf{x}[\mathcal{L}_{p_\theta}(\mathbf{x})] &= \mathbb{E}_{\mathbf{x}_1}[\mathcal{L}_{p_\theta}(\mathbf{x}_1)] + \mathbb{E}_{\mathbf{x}_1} \mathbb{E}_{(\mathbf{x}_2 \dots \mathbf{x}_{s+1})}[\mathcal{L}_{p_\theta}((\mathbf{x}_2 \dots \mathbf{x}_{s+1})) | \mathbf{x}_1] \\ &= \mathbb{E}_{\mathbf{x}_1}[\mathcal{L}_{p_\theta}(\mathbf{x}_1)] + \sum_{\mathbf{x}_1} p(\mathbf{x}_1) \sum_{(\mathbf{x}_2 \dots \mathbf{x}_{s+1})} p(\mathbf{x}_2 \dots \mathbf{x}_{s+1} | \mathbf{x}_1) \cdot \mathcal{L}_{p_\theta}((\mathbf{x}_2 \dots \mathbf{x}_{s+1})) \\ &= \mathbb{E}_{\mathbf{x}_1}[\mathcal{L}_{p_\theta}(\mathbf{x}_1)] + \mathbb{E}_{(\mathbf{x}_2 \dots \mathbf{x}_{s+1})}[\mathcal{L}_{p_\theta}((\mathbf{x}_2 \dots \mathbf{x}_{s+1}))] \\ &= \sum_{k=1}^{s+1} \mathbb{E}_{\mathbf{x}_k}[\mathcal{L}_{p_\theta}(\mathbf{x}_k)] \\ &= \left\lceil \frac{|\mathbf{x}|}{d} \right\rceil \left[- \sum_{l=1}^d \sum_{j=1}^{2^{l-1}} p_{lj} \log p_{lj} \right], \end{aligned}$$

thus the proof is completed. \square

Definition B.2 (Mass Distribution in Token Tree). Consider the sample space Ω consisting of all responses in dataset \mathcal{D} . The probability distribution $\mathcal{P}_\mathcal{D}$ of all subtrees at the d -th level nodes of $\mathcal{T}_\mathcal{D}$ is a mapping from Ω to $[0, 1]$. Let $X_\mathcal{D}$ be the random variable representing the probability value taken at each leaf. The mass distribution P_{mass} represents the probability that $X_\mathcal{D}$ takes the corresponding probability value. According to the definition of P_{mass} , $\mathbb{E}[X_\mathcal{D}] = 1$.

Remark B.3 (Mixture of Mass Distribution). For independently and differently distributed datasets $\mathcal{D}_1, \dots, \mathcal{D}_N$, $\mathcal{D} = \bigcup_{i=1}^N \mathcal{D}_i$ is a mixture of these datasets. For the pruned trees $\mathcal{T}_1, \dots, \mathcal{T}_N$ of these datasets with depth d , the random variables of their leaf nodes satisfy the following relationship:

$$X_{\mathcal{D}} = \frac{\sum_{k=1}^N |\mathcal{D}_k| X_{\mathcal{D}_k}}{\sum_{k=1}^N |\mathcal{D}_k|},$$

where $X_{\mathcal{D}_k}$ follows the mass distribution \mathcal{P}_{mass}^k . For $X_{\mathcal{D}_{k_i}}$ and $X_{\mathcal{D}_{k_j}}$ from different datasets, $X_{\mathcal{D}_{k_i}}$ and $X_{\mathcal{D}_{k_j}}$ are independent of each other.

Lemma B.4 (Entropy of Mass Distribution). *Consider the pruned trees \mathcal{T}'_k and \mathcal{T}' of dataset \mathcal{D}_k and $\mathcal{D} = \bigcup_{i=1}^N \mathcal{D}_i$. Denote that the response distribution and the mass distribution of \mathcal{T}' 's tree nodes are $\mathcal{P}^{\mathcal{D}}$ and \mathcal{P}_{mass} . Similarly, we define the response distribution $\mathcal{P}_k^{\mathcal{D}}$ and the mass distribution is \mathcal{P}_{mass}^k . When the number of the leaf nodes M is sufficiently large, the Shannon entropy of the response distribution can be rewritten as follows.*

$$\mathbb{E}_{\mathbf{x} \sim \mathcal{P}_k} [-p^{\mathcal{D}_k} \log p^{\mathcal{D}}] = \mathbb{E}_{X_{\mathcal{D}_k} \sim \mathcal{P}_{mass}^k, X_{\mathcal{D}} \sim \mathcal{P}_{mass}} [-X_{\mathcal{D}_k} \log X_{\mathcal{D}}] + \log M,$$

where $p^{\mathcal{D}}$, $p^{\mathcal{D}_k}$ stand for the probability of the leaf nodes of \mathcal{T}' , \mathcal{T}'_k while $X_{\mathcal{D}_k}$, $X_{\mathcal{D}}$ stand for the random variables of the probability of the leaf nodes of \mathcal{T}' , \mathcal{T}'_k .

Proof. Let M be the number of leaf nodes of \mathcal{T}' . According to the definitions of the response distribution \mathcal{P} and mass distribution \mathcal{P}_{mass} , we have $M p^{\mathcal{D}_j} = X_{\mathcal{D}_j}$, $\forall j \in \{1, \dots, N\}$. Therefore,

$$\begin{aligned} \mathbb{E}_{\mathbf{x} \sim \mathcal{P}_k} [-p^{\mathcal{D}_k} \log p^{\mathcal{D}}] &= \sum_{i=1}^M -p_i^{\mathcal{D}_k} \log p_i^{\mathcal{D}} \\ &= \sum_{i=1}^M -\frac{1}{M} X_{i, \mathcal{D}_k} \log X_{i, \mathcal{D}_k} + \log M \\ &= \mathbb{E}_{X_{\mathcal{D}_k} \sim \mathcal{P}_{mass}^k, X_{\mathcal{D}} \sim \mathcal{P}_{mass}} [-X_{\mathcal{D}_k} \log X_{\mathcal{D}}] + \log M. \end{aligned}$$

□

Remark B.5. In Lemma B.4, $X_{\mathcal{D}_k}$ are assumed to be independent. However due to $\sum_{i=1}^M p_i^{\mathcal{D}_k} = 1$, the $X_{\mathcal{D}_k}$ are not actually independent. Considering that M is sufficiently large in our subsequent analysis, we can regard the independence of $X_{\mathcal{D}_k}$ as a good approximation.

We assume that the mass distribution of the segment follows a heavy-tailed Pareto distribution, with supporting evidence from (Mingard et al., 2021; Zipf, 1946)

Assumption B.6 (The Pareto Distribution). We assume that the mass distribution of pruned token trees \mathcal{T} of depth d , across different datasets, follows a Pareto distribution with identical parameters:

$$p_X(x) = \begin{cases} \frac{\alpha c^\alpha}{x^{\alpha+1}} & x \geq c, \\ 0 & x < c, \end{cases}$$

where α, c are parameters of the Pareto distribution. Here we assume that α, c is sufficiently large due to the lighter heavy-tailed nature of the mass distribution.

Theorem B.7 (Elasticity of Language Models). Consider datasets \mathcal{D}_1 , \mathcal{D}_2 and perturbation \mathcal{D}_3 each with a Pareto mass distribution (Newman, 2005), and the model $p_\theta(\cdot)$ trained on $\mathcal{D} = \mathcal{D}_1 \cup \mathcal{D}_2 \cup \mathcal{D}_3$. When dataset \mathcal{D}_3 's data volume $|\mathcal{D}_3|$ changes, the normalized compression rates $\gamma_{p_\theta}^{\mathcal{D}_1/\mathcal{D}}$ and $\gamma_{p_\theta}^{\mathcal{D}_2/\mathcal{D}}$ satisfies:

$$\begin{aligned} \frac{d\gamma_{p_\theta}^{\mathcal{D}_2/\mathcal{D}}}{dl} &= \Theta \left(k \frac{d\gamma_{p_\theta}^{\mathcal{D}_1/\mathcal{D}}}{dl} \right), \\ \frac{d\gamma_{p_\theta}^{\mathcal{D}_1/\mathcal{D}}}{dl} &> 0, \frac{d\gamma_{p_\theta}^{\mathcal{D}_2/\mathcal{D}}}{dl} > 0, \end{aligned} \quad (4)$$

where $l = \frac{|\mathcal{D}_3|}{|\mathcal{D}_2|} \ll 1$, $k = \frac{|\mathcal{D}_1|}{|\mathcal{D}_2|} \gg 1$.

Proof. For the sake of convenience in calculations, we first use Lemma B.4 to replace the Shannon entropy of response distribution.

$$\begin{aligned} \frac{d\gamma_{p_\theta}^{\mathcal{D}_j/\mathcal{D}}}{dl} &= - \frac{d \left(\mathbb{E}_{\mathbf{x} \sim \mathcal{P}_j} [-p^{\mathcal{D}_j} \log p^{\mathcal{D}}] - \log M \right)}{dl} \\ &= - \frac{d \left(\mathbb{E}_{X_{\mathcal{D}_j} \sim \mathcal{P}_{mass}^j, X_{\mathcal{D}} \sim \mathcal{P}_{mass}} [-X_{\mathcal{D}_j} \log X_{\mathcal{D}}] \right)}{dl}. \end{aligned}$$

According to Assumption B.6, $X_{\mathcal{D}_j}$ follows a Pareto distribution with the parameters α and c . Hence,

$$\begin{aligned} &\mathbb{E}_{X_{\mathcal{D}_j} \sim \mathcal{P}_{mass}^j, X_{\mathcal{D}} \sim \mathcal{P}_{mass}} [-X_{\mathcal{D}_j} \log X_{\mathcal{D}}] \\ &= - \int_c^{+\infty} \int_c^{+\infty} \int_c^{+\infty} \frac{\alpha^3 c^{3\alpha} x_j}{\prod_{i=1}^3 x_i^{\alpha+1}} \log \frac{\sum_{i=1}^3 |\mathcal{D}_i| x_i}{\sum_{i=1}^3 |\mathcal{D}_i|} dx_1 dx_2 dx_3 \\ &= - \int_c^{+\infty} \int_c^{+\infty} \int_c^{+\infty} \frac{\alpha^3 c^{3\alpha} x_j}{\prod_{i=1}^3 x_i^{\alpha+1}} \log \frac{kx_1 + x_2 + lx_3}{k+l+1} dx_1 dx_2 dx_3 \end{aligned}$$

where $j = 1, 2, 3$. Therefore, $\frac{d\gamma_{p_\theta}^{\mathcal{D}_1/\mathcal{D}}}{dl}$ and $\frac{d\gamma_{p_\theta}^{\mathcal{D}_2/\mathcal{D}}}{dl}$ can be written as:

$$\frac{d\gamma_{p_\theta}^{\mathcal{D}_1/\mathcal{D}}}{dl} = \alpha^3 c^{3\alpha} \frac{dS_1}{dl}, \quad (5)$$

$$\frac{d\gamma_{p_\theta}^{\mathcal{D}_2/\mathcal{D}}}{dl} = \alpha^3 c^{3\alpha} \frac{dS_2}{dl} \quad (6)$$

where

$$\begin{aligned} S_1 &= \int_c^{+\infty} \int_c^{+\infty} \int_c^{+\infty} \frac{1}{x_1^\alpha x_2^{\alpha+1} x_3^{\alpha+1}} \log \frac{kx_1 + x_2 + lx_3}{k+l+1} dx_1 dx_2 dx_3 \\ S_2 &= \int_c^{+\infty} \int_c^{+\infty} \int_c^{+\infty} \frac{1}{x_1^{\alpha+1} x_2^\alpha x_3^{\alpha+1}} \log \frac{kx_1 + x_2 + lx_3}{k+l+1} dx_1 dx_2 dx_3. \end{aligned}$$

Proving that $\frac{d\gamma_{p_\theta}^{\mathcal{D}_2/\mathcal{D}}}{dl} = \Theta \left(k \frac{d\gamma_{p_\theta}^{\mathcal{D}_1/\mathcal{D}}}{dl} \right)$ is equivalent to proving:

$$\lim_{k \rightarrow +\infty, l \rightarrow 0} \frac{k \cdot \frac{d\gamma_{p_\theta}^{\mathcal{D}_1/\mathcal{D}}}{dl}}{\frac{d\gamma_{p_\theta}^{\mathcal{D}_2/\mathcal{D}}}{dl}} = C, \quad (7)$$

where C is a constant. By substituting (5) and (6) into (7), we have

$$\lim_{k \rightarrow +\infty, l \rightarrow 0} \frac{k \cdot \frac{d\gamma_{p\theta}^{\mathcal{D}_1/\mathcal{D}}}{dl}}{\frac{d\gamma_{p\theta}^{\mathcal{D}_2/\mathcal{D}}}{dl}} = \frac{\lim_{k \rightarrow +\infty, l \rightarrow 0} k \left(\frac{dS_1}{dl} \right)}{\lim_{k \rightarrow +\infty, l \rightarrow 0} \frac{dS_2}{dl}}. \quad (8)$$

Now calculate the values of $\frac{dS_1}{dl}$ and $\frac{dS_2}{dl}$ respectively in the case of $k \rightarrow +\infty, l \rightarrow 0$.

$$\begin{aligned} & \lim_{k \rightarrow +\infty, l \rightarrow 0} \frac{dS_1}{dl} \\ &= \lim_{k \rightarrow +\infty, l \rightarrow 0} \int_c^{+\infty} \int_c^{+\infty} \int_c^{+\infty} \frac{(k+1)x_3 - kx_1 - x_2}{x_1^\alpha x_2^{\alpha+1} x_3^{\alpha+1} (k+l+1)(kx_1+x_2+lx_3)} dx_1 dx_2 dx_3 \\ &= \int_c^{+\infty} \int_c^{+\infty} \lim_{k \rightarrow +\infty, l \rightarrow 0} \int_c^{\delta(kx_1+x_2)} \frac{1}{x_1^\alpha x_2^\alpha x_3^\alpha (kx_1+x_2+lx_3)} \\ &\quad - \lim_{k \rightarrow +\infty, l \rightarrow 0} \int_c^{+\infty} \int_c^{+\infty} \int_c^{+\infty} \frac{1}{x_1^\alpha x_2^{\alpha+1} x_3^{\alpha+1} (k+1+l)} dx_1 dx_2 dx_3 \\ &= \lim_{k \rightarrow +\infty, l \rightarrow 0} \int_c^{+\infty} \int_c^{+\infty} \int_c^{+\infty} \frac{1}{x_1^\alpha x_2^{\alpha+1} x_3^\alpha \theta'_1 k x_1} dx_1 dx_2 dx_3 \\ &\quad - \lim_{k \rightarrow +\infty, l \rightarrow 0} \frac{1}{(k+1)\alpha^2(\alpha-1)c^{3\alpha-1}} \\ &\hspace{25em} \text{where } \theta' \rightarrow 1 \\ &= \lim_{k \rightarrow +\infty, l \rightarrow 0} \int_c^{+\infty} \int_c^{+\infty} \int_c^{+\infty} \frac{1}{kx_1^{\alpha+1} x_2^{\alpha+1} x_3^\alpha} dx_1 dx_2 dx_3 \\ &\quad - \lim_{k \rightarrow +\infty, l \rightarrow 0} \frac{1}{(k+1)\alpha^2(\alpha-1)c^{3\alpha-1}} \\ &= \frac{1}{k(k+1)\alpha^2(\alpha-1)c^{3\alpha-1}}. \end{aligned} \quad (9)$$

Using the same technique as for calculating S_1 , we can similarly obtain

$$\lim_{k \rightarrow +\infty, l \rightarrow 0} \frac{dS_2}{dl} = \frac{k + \alpha^2}{k(k+1)\alpha^2(\alpha-1)^2(\alpha+1)c^{3\alpha-1}},$$

As a result, Equation (8) can be written as:

$$\lim_{k \rightarrow +\infty, l \rightarrow 0} \frac{k \cdot \frac{d\gamma_{p\theta}^{\mathcal{D}_1/\mathcal{D}}}{dl}}{\frac{d\gamma_{p\theta}^{\mathcal{D}_2/\mathcal{D}}}{dl}} = \lim_{k \rightarrow +\infty, l \rightarrow 0} \frac{k \cdot \frac{1}{k(k+1)\alpha^2(\alpha-1)c^{3\alpha-1}}}{\frac{k+\alpha^2}{k(k+1)\alpha^2(\alpha-1)^2(\alpha+1)c^{3\alpha-1}}} = \alpha^2,$$

where α^2 is a constant. Thus, the proof is completed.

Next, we prove that $\frac{d\gamma_{p\theta}^{\mathcal{D}_1/\mathcal{D}}}{dl} > 0$,

$$\frac{d\gamma_{p\theta}^{\mathcal{D}_1/\mathcal{D}}}{dl} = \lim_{k \rightarrow +\infty, l \rightarrow 0} \alpha^3 c^{3\alpha} \frac{dS_1}{dl} = \frac{\alpha c}{k(k+1)(\alpha-1)} > 0.$$

Similarly, due to k is sufficiently large, we have

$$\frac{d\gamma_{p\theta}^{\mathcal{D}_2/\mathcal{D}}}{dl} = \lim_{k \rightarrow +\infty, l \rightarrow 0} \alpha^3 c^{3\alpha} \frac{dS_2}{dl} = \frac{\alpha c(k + \alpha^2)}{k(k+1)(\alpha-1)^2(\alpha+1)} > 0.$$

□

C Ablation Study

To further verify the existence of model *elasticity* and the generality of its relationship with model size and pre-training data volume, we conducted experiments with different fine-tuning algorithms (DPO (Rafailov et al., 2024)), broader scales of pre-training data volume, and larger sizes of pre-trained models.

DPO Finetuning Experiments on LLMs *Elasticity*. We used the RLHF algorithm (Ouyang et al., 2022), specifically DPO (Rafailov et al., 2024), to fine-tune large language models in order to observe the *elasticity* of the models. The experimental procedure consists of the following two steps: 1) Perform SFT on the pre-trained model using various levels of positive sample data. 2) Use various levels of negative sample data, where negative samples are used as chosen responses and positive samples as rejected responses, to apply DPO for *inverse alignment* on the positively aligned model.

The experimental results are shown in Figure 7 and Figure 8. The results indicate that under DPO fine-tuning, LLMs continue to exhibit *elasticity* in style generation tasks. Additionally, as the model size and the amount of pre-training data increase, the model’s *elasticity* shows an enhancing trend, which is consistent with the conclusions in Figures 5 and Figure 6. This suggests that differences in fine-tuning alignment algorithms do not affect the *elasticity* of language models.

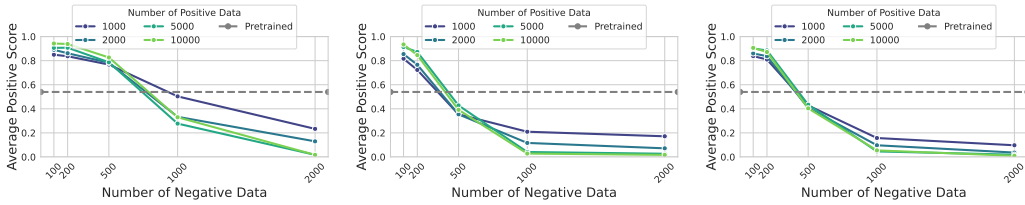


Figure 7: **DPO Finetuning Experiments on IMDb.** Each subfigure from left to right shows the changes in LLMs with parameter sizes of 0.5B, 4B, and 7B.

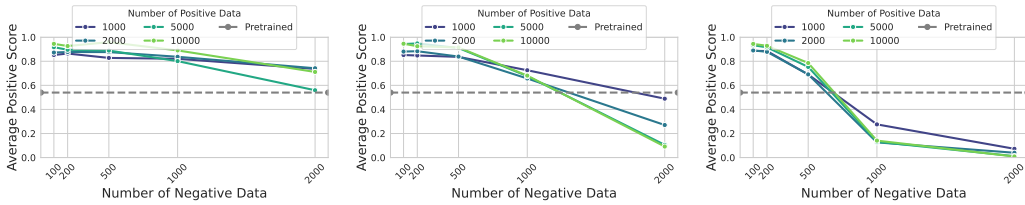


Figure 8: **DPO Finetuning Experiments on IMDb.** Each subfigure from left to right shows the changes in pre-training data volume of 2.0T, 2.5T, and 3.0T.

Reverse Finetuning Experiments on LLMs *Elasticity*. To eliminate the influence of positive data on model *elasticity* experimental results, we adopted a reverse experimental setup: we use negative data during the SFT stage and use positive data during *inverse alignment* stage. The experimental results are shown in Figure 9. The results indicate that *elasticity* in language models is still observed in the reverse experiments, showing a trend where larger model sizes correspond to greater *elasticity*, consistent with the results in Figure 5.

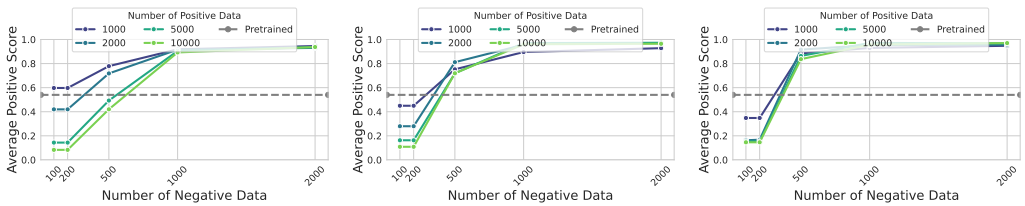


Figure 9: **Reverse Fine-tuning Results on IMDb.** Each subfigure from left to right shows the changes in LLMs with parameter sizes of 0.5B, 4B, and 7B, respectively.

Pre-training Data Volume Experiments on LLMs *Elasticity*. We present the experimental results for a broader range of pre-training data volumes in Figure 10. When the pre-training data volume is 0.1T, 0.5T, and 1.0T, the model still demonstrates the phenomenon that *elasticity* increases with the volume of pre-training data, which is consistent with the results reported in Figure 6, where the pre-training data volumes range from 2.0T to 3.0T.

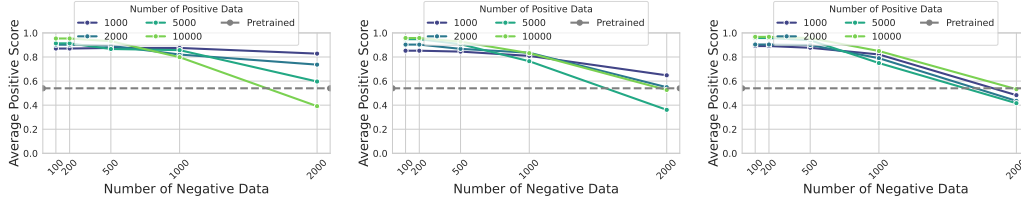


Figure 10: **Experimental Results on IMDb.** Each subfigure from left to right shows the changes in pre-training data volumes of 0.1T, 0.5T, and 1.0T.

Model Size Scale Experiment on LLMs *Elasticity*. To examine whether the *elasticity* phenomenon in language models is independent of model parameter size, we conducted experiments on the larger parameter-scale model, Qwen1.5 72B (Bai et al., 2023). The experimental results are shown in Figure 11. The results indicate that even models with larger parameter sizes still exhibit the *elasticity* phenomenon, demonstrating that the presence of *elasticity* is not dependent on the size of the model parameters.

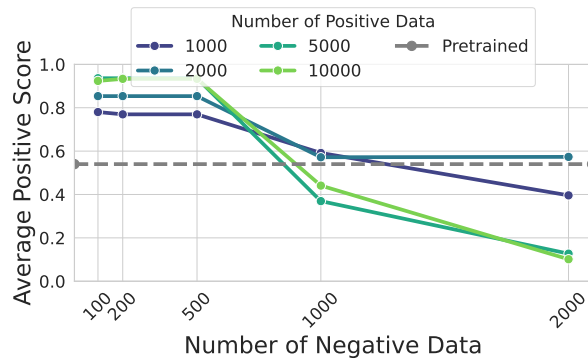


Figure 11: **Experimental Results on IMDb with Qwen1.5 72B.**